SCIENTIFIC REPORTS

OPEN

SUBJECT AREAS:
BATTERIES
IMAGING TECHNIQUES
SYNTHESIS AND PROCESSING

Received
16 September 2013

Accepted
30 October 2013

Published
15 November 2013

Correspondence and requests for materials should be addressed to H.M.Z. (hmzheng@lbl.gov)

* These authors contributed equally to this work.

Structural and Morphological Evolution of Lead Dendrites during Electrochemical Migration

Minghua Sun[1]*, Hong-Gang Liao[1]*, Kaiyang Niu[1]* & Haimei Zheng[1,2]

[1]Materials Sciences Division, Lawrence Berkeley National Laboratory, Berkeley CA 94720 US, [2]Department of Materials Science and Engineering, University of California, Berkeley CA 94720 US.

The electrochemical deposition and dissolution of lead on gold electrodes immersed in an aqueous solution of lead nitrate were studied in situ using a biasing liquid cell by transmission electron microscopy (TEM). We investigate in real time the growth mechanisms of lead dendrites as deposited on the electrodes under an applied potential. TEM images reveal that lead dendrites are developed by the fast protrusion of lead branches in the electrolyte and tip splitting. And, the fast growing tip of the dendritic branch is composed of polycrystalline nanograins and it develops into a single crystalline branch eventually. This study demonstrated unique electrochemical growth of single crystal dendrites through nucleation, aggregation, alignment and attachment of randomly oriented small grains. Additionally, we found the lead concentration in the electrolyte drastically influences the morphology of dendritic formation.

An understanding of the growth mechanisms of metal dendrites during an electrochemical process is of significant importance to improving the life time of batteries or electronic devices. For instance, during the operation of lead-acid, zinc-air or lithium ion batteries, the repeated charge and discharge often lead to deposition of metal dendrites on the electrode (anode), which can result in short-circuit between the two electrodes thus failure of the batteries[1]. Dendritic growth of metals is also one of the major failure mechanisms in electronic packaging[2]. There has been a lot of effort in reducing metal dendrite formation and uncovering the mechanisms of dendritic growth.

Dendritic growth is ubiquitous in materials solidification and crystallization. Its complexity characterized as multilevel branching has attracted abroad of interests over the years[3–14]. It has been identified that dendrite formation arises from the instabilities when the growth rate is limited by the diffusion rate of ions from the solution to the interface. Granasy et al.[15] using a phase-field model described that the randomly distributed particle inclusions perturb the crystallization by deflecting the tips of the growing dendrite arms. Thus, polycrystalline dendrites or fractal patterns can be achieved. Fang et al.[16] reported the double-interface growth of silver in a replacement reaction where the dendrite formation was controlled by the growth of an amorphous phase and the subsequent crystallization of the amorphous structure. It has also been reported that the dendrites can emerge from aggregation[17] or oriented attachment[18] of nanoparticles. So far, significant effort has been made and progress has been achieved in the understanding of dendritic growth, however, there is no consensus on the mechanisms of nucleation, crystallization and branching of dendrites from electrochemical deposition mainly due to the lack of direct observation.

Real time monitoring the electrochemical processes with high spatial resolution using transmission electron microscopy (TEM) provides the opportunity to elucidate the mechanisms of growth. Imaging of liquid samples using TEM with sub-nanometer resolution has been achieved assisted by the development of liquid cells. A well-sealed liquid cell can maintain a small amount of liquids inside the cell for an extended period of time under the high-vacuum environment. An electrochemical process can be studied with the electrodes built inside the liquid cell (an electrochemical liquid cell). In-situ TEM study of the electrochemical deposition of Ni[19], Cu[20], Pb[21], Ag[22], etc. on electrodes has been reported previously. In this work, we designed and fabricated the electrochemical liquid cells with improved spatial resolution by using thinner membranes, which allows us to study dendritic growth in situ with an unprecedented level of details. Additionally, the electrode has a limited area of exposure to the electrolyte so that the electrochemical processes are localized. The electrochemical liquid cell design is shown

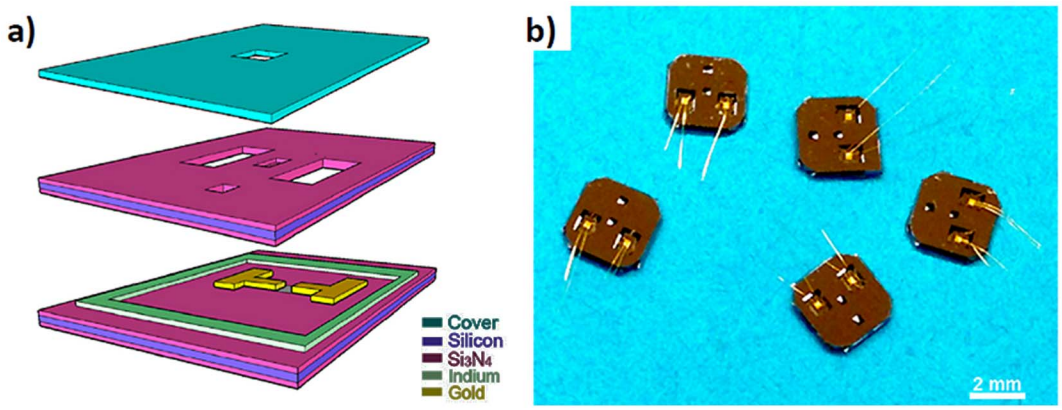

Figure 1 | Home-made electrochemical liquid cells. (a) A schematic diagram of an electrochemical liquid cell; (b) A photo of the assembled electrochemical liquid cells.

in Figure 1, which allow an electric bias to be applied between the two electrodes for the in situ electrochemical TEM experiments.

We study the electrochemical deposition and dissolution of lead metal dendrites on gold electrodes immersed in an aqueous solution of lead nitrate. Different concentration of lead ions, i.e., 100 mg/mL or 5 mg/mL, dissolved in water was used. And, the effects of surfactants, triethylene glycol were evaluated by changing the ratio of triethylene glycol to water from 4 : 1 to 3 : 2. The cyclic electric potential of −0.8 to 1.2 V was applied between two electrodes (Figure S1). The crystallization and the morphology evolution of lead dendritic structures were investigated using both in-situ and ex-situ TEM characterizations. The influences of electrolyte concentration, electric field and surfactants on the dendritic growth were discussed.

Results

We track the trajectories of deposition and dissolution of lead dendrites on the electrodes during the charge cycles. The sequential images show the development of dendritic structure by tip splitting at a constant bias of −0.8 V and the subsequent dissolution of the dendrites when the bias was revised to 1.2 V (Figure 2(a), Figure S2 and Movie S1). Under the electric bias, a lead needle is formed and it rapidly develops into branched structure. Each new branch grows fast approximately along the direction of the electric field. The growth speed decreases drastically as the tip splits. The speed of growth is correlated with the shape changes of the tip. The shape evolution of each individual branches is shown in Figure 2(b), where seven branches are highlighted. The fast growing branch has a sharper tip. The growth speed decreases as the tip becomes thicker and rounded. The fast growth also leads to tip splitting (Figure 2(d)). For instance, the fast growing branches (i.e., branch 1., 3. and 7.) split and develop new branches. However, branches 2., 4. and 6. get rounded and they did not split. When the curvature (radius) of the tip is below 45 nm the tip is unstable thus split. Additionally, the branch development is asymmetric, which can result from the local inhomogeneity and fluctuations during growth.

The fast development of dendrites can lead to breakdown of the electrochemical cell. Dendrites protrude into the electrolyte and the thin branches form the backbone then become much thicker. They continue to grow until two electrodes are connected (Figure S3). Then, the device stops responding to the applied bias. However, before shortage, if the electric bias is reversed the dendrites can shrink and collapse. As shown in Figure 2(a–c), branches 2., 4., 6. and 7. become thinner and shorter simultaneously, while branches in the middle of the dendrites (i.e., branch 1., 3. and 5.) have no obvious changes of their length while getting thinned down.

The growth and dissolution of a needle without tip splitting are shown in Figure 3(a). We track the evolution of the tip curvature and growth rate. Initially, a small cluster is developed on the electrode (as indicated by an arrow in Figure 3(a)). The tip gets sharper during the growth and eventually a needle with dimensions of 4 × 1 μm is achieved. In the next 20 seconds, the length of the needle maintains constant while the tip becomes rounded. When the electric bias is reversed, the length of the needle suddenly reduces about 600 nm. It is followed by the slow decrease while the tip becomes sharper and sharper. In the last 20 seconds, both the length and width of the tip reduces rapidly until it is completely dissolved. It is noted that under the revised bias, some dendrites can be disconnected from the electrode before the branches are dissolved (Figure S4). The residue of Pb dendrites stays in the solution and it can not be dissolved. Such loss of mass during electrochemical processes can be an important issue, for example, it can lead to degradation of rechargeable Li batteries[1].

We found the precursor concentration has significant effects on the morphology of the dendrites. As the Pb ion concentration changes from 100 mg/mL to 5 mg/mL, the average dimensions (d × L) of the branches reduce from 500 × 3000 nm to 100 × 480 nm and the growth rate of the dendritic front increases about 10 times (Figure 4(a) and 4(b)). The number of branches from the lower concentration solution is much higher. In both cases, the general growth direction is aligned with the electric field. And, the inhomogeneous growth along the electrode has been observed. Faster growth and larger dendrites are observed at the corner of the electrode, where the electric field is expected to be stronger.

To demonstrate the growth and crystallization mechanisms of the dendrites, we also did ex-situ experiments. The same electrochemical cells were used without sealing the cell and dendrites were taken from the electrodes in the open reservoirs and put onto the carbon sample grids for TEM studies. Extensive studies confirm that the tips of the dendrites are polycrystalline. As shown in the selected area electron diffraction (SAED) pattern of a dendritic branch (Figure 5(a)), it has the face centered cubic (FCC) structure with no preferred orientation. Dark field image of the front part of the branch shows that it is composed of rice shaped grains with 10–20 nm in diameter and 30–50 nm long (Figure 5(b)). Interestingly, the main part of the branch is close to single crystalline with the long axis along [100] direction (Figure 5(c–f)). Figure 5(f) is the dark field image of a (200) grain that is almost across the whole branch with the dimensions of 200 nm × 500 nm.

Based on the above observation, we propose a novel electrochemical growth model as below. As shown in Figure 6, the electrochemically reduced metal forms nanograins on the electrode initially. As the deposition continues, those nanograins aggregate into a cluster with polycrystalline features. The cluster can grow rapidly along the electric field and form a needle. Subsequently, reconstruction and coalescence of the polygrains occur and eventually single crystalline structure is achieved. It is likely that the rice shaped grains preferably rotate along <100> orientation thus the needle is <100> oriented

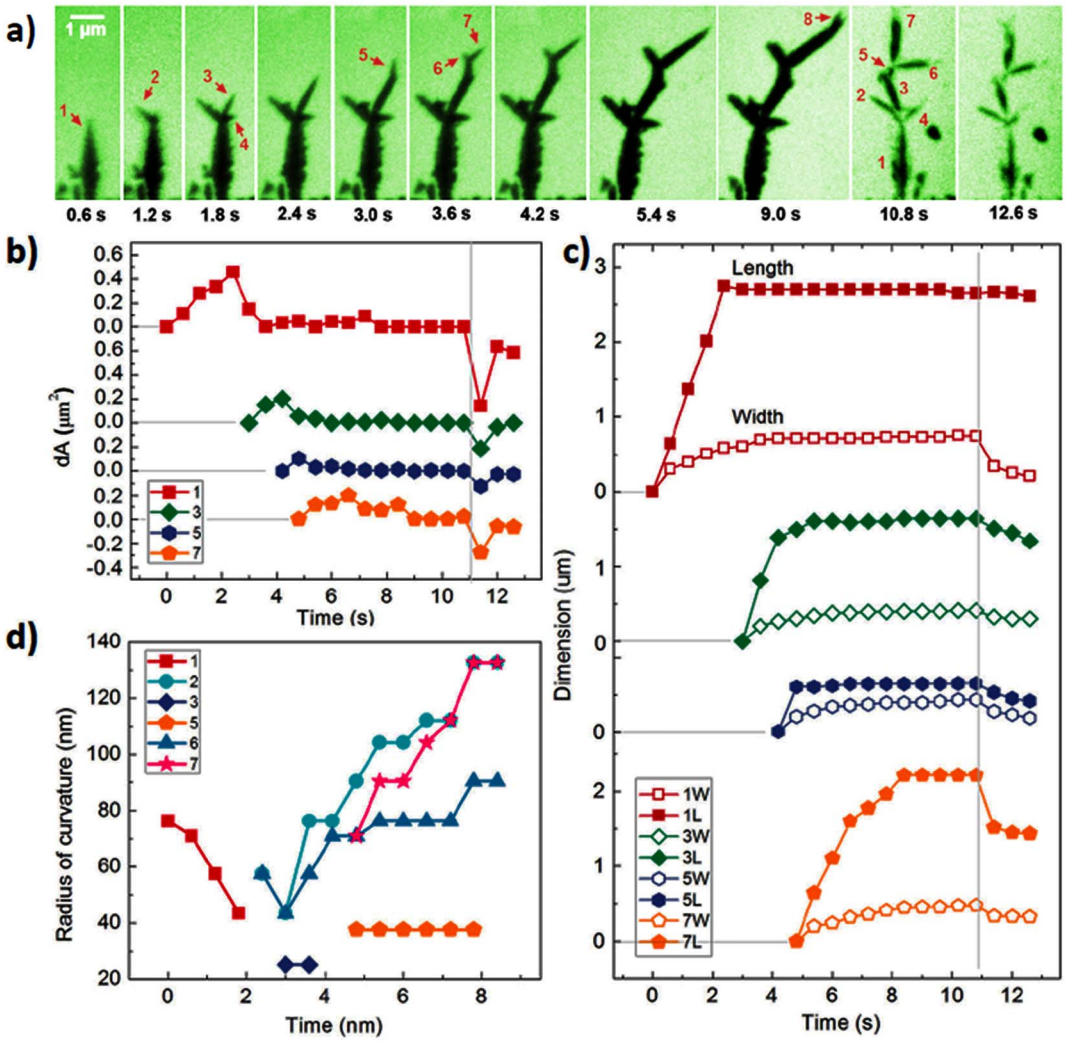

Figure 2 | Trajectories of lead dendrites during growth and dissolution. (a) Time series of TEM images showing growth and dissolution of Pb dendrites; (b) Area changes of five selected branches versus time; (c) Length and width changes of each individual branch as a function of time; (d) Sharpness changes of the tip as a function of time.

along the long axis. It is expected that there are local inhomogeneities at the growth front. The tip splitting or branching is likely from the fluctuations in local environment. For example, clusters can nucleate on the surface of a dendritic branch and grow into a new branch depending on the local composition, electric field and so on. The growth of new branches can follow the same growth mode that it starts from polycrystalline then transforms into single crystalline with the long axis along <100> direction. Such a branching mechanism is consistent with our observation that the main branch of the dendrites and the secondary branches are all in <100> direction but they are not perpendicular with each other. Our proposed dendritic tip splitting due to fluctuations agrees with Granasy et al.[15] that randomly distributed particle inclusions perturb the crystallization by deflecting the tips of the growing dendrite arms. However, the structural transition of a dendritic branch from polycrystalline to a single crystal during electrochemical deposition has not been reported before.

We expect surfactants play a role in the electrochemical deposition of Pb. Here, triethylene glycol with different concentration has been used. The dendrite morphologies are different from those grown in pure water where single crystal dendrites were achieved directly during growth[21]. However, there is no obvious change in the growth of Pb dendrites as the triethylene glycol concentration is changed from 80% to 60%. Future studies with more systematic change of surfactant concentration as well as ligand length will be helpful to elucidate the role of surfactants.

Discussion

Electron beam has perceptible effects on in situ electrochemical TEM experiments. Besides the reduction of metal precursor[23–25], electron beam can produce bubbles in liquids, generate solvated ions or electrons and rupture the liquid film[26,27]. During the growth of Pb dendrites, bubbles are formed at solid-liquid interfaces as well as in the liquid electrolyte (Figure S5(a) and S5(b)). Radiolysis of water in the aqueous electrolyte can generate hydrogen and oxygen bubbles, which grow and migrate in the solution[27]. However, growth and shrinkage of some bubbles are synchronized with the Pb dendrite deposition (Figure S5(b)), which suggests these bubbles are likely generated from electrolysis of water (electrolyte decomposition by the applied electric bias) rather than radiolysis alone. We measure the electric current between two electrodes by periodically blocking the electron beam. Significant increase (4.5 times) in the current is observed, see C-V (current-voltage) plot in Figure S6. This is probably because a large number of free radicals and/or solvated electrons are generated as the electron beam passes through the liquids. In principle the solvated electrons can reduce Pb^{2+} ions in the electrolyte, which could introduce precipitation of Pb in the electrolyte solution. However, under the current imaging conditions with the

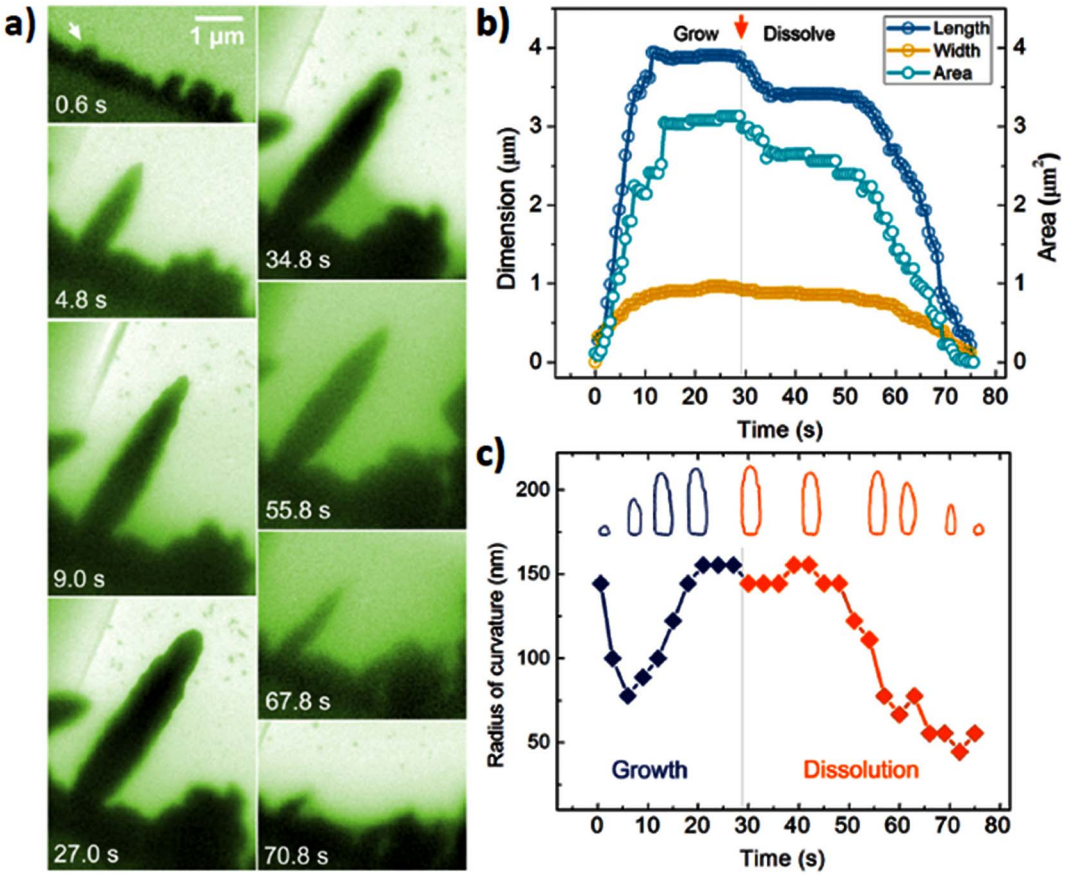

Figure 3 | Size and shape evolution of a lead needle during a charge cycle. (a) Sequential images showing growth and dissolution of a lead branch; (b) Changes of length, width and area of the lead tip as a function of time; (c) Sharpness evolution of the lead tip. Inset is the corresponding contour maps of this tip along the trajectory.

electron current density (about 5×10^2 electrons$\cdot s^{-1}\cdot Å^{-2}$), no obvious precipitation of Pb particles or clusters is observed in the solution. Although electron beam effects are complex and hard to quantify, our extensive experiments both in situ and ex situ (without electron beam) show that such dendritic growth of Pb can be achieved only when an electric bias is applied in the electrochemical cell. In order to more quantitatively understand the role of electron beam theoretical modeling of electrochemical processes is needed, as reported recently by Longo et al.[28].

In summery, we have studied lead dendritic growth in situ under TEM using a home-made biasing electrochemical liquid cell. Tracking the structural and shape evolution of the dendrites in real time reveals the growth and tip splitting dynamics and characteristics. Our experimental results demonstrate that the reduction of lead ions on the electrode can induce nucleation and aggregation of randomly oriented small grains. The cluster rapidly grows into a rod or a needle along the electric field. While the fast growing tip maintains polycrystalline features, those small grains can rearrange and form a single crystal later in the main part of the needle. A new branch may not be perpendicular to the main branch although they are all oriented along <100> along long axis. We show that ion concentration in the electrolyte drastically influences the morphology and growth rate of the dendrites. It is noted that the dendrites morphology and growth dynamics can be affected by the thickness of thin

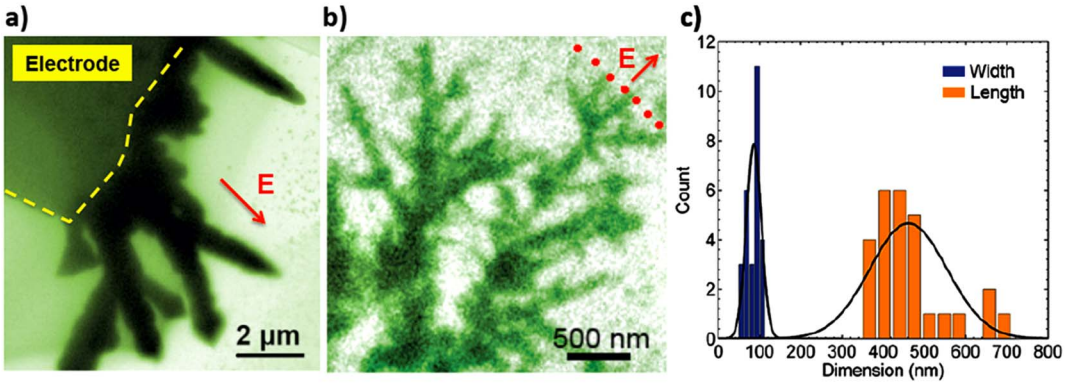

Figure 4 | Effects of lead ion concentration in the precursor solution on the dendrite morphology. (a) A snapshot image of lead electro-deposited on the electrode from the solution with lead concentration of 100 mg/mL; (b) A snapshot image of lead electro-deposited on the electrode from the solution with lead concentration of 5 mg/mL; (c) Statistic width and length of the branches in b.

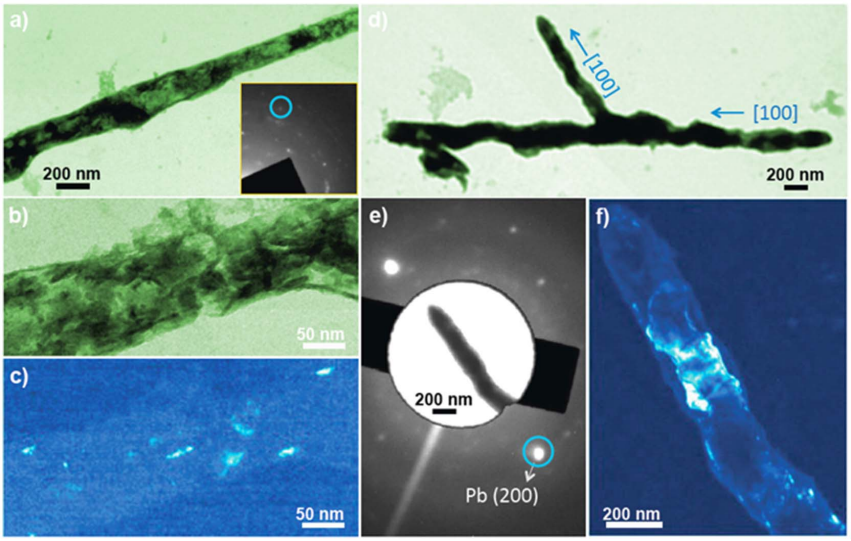

Figure 5 | Ex-situ study of as-formed lead branches. (a) Low magnification TEM image of a lead needle. The inset is the corresponding selected area electron diffraction (SAED) pattern; (b) High magnification TEM image of the needle in a; (c) Dark field TEM image of the branch in b; (d) Low magnification TEM image of a lead dendrite; (e) SAED pattern of a branch in d; The inset is an image of the lead branch corresponding to the diffraction pattern with matching crystal graphic orientation; (f) Dark field TEM image of the branch showing the (200) plane (grain).

liquid. However, no pronounced differences in dendrites grown from ex situ experiments and from in situ experiments with the liquid layer of 150 nm or thicker. Additionally, although electron beam has noticeable effects on the electrolyte by creating free radicals, solvated electrons, bubbles, etc., dendritic growth of Pb happens under an applied electric bias with key electrochemistry features. This work provides some reference points for the future study of electrochemical processes under TEM investigations.

Methods

We developed a self-contained electrochemical liquid cell for in situ TEM studies. A schematic of the biasing liquid cell is shown in Figure 1. We fabricated the biasing cells at the Marvell Nanofabrication Laboratory of the University of California at Berkeley. The bottom, top and cover chips of the biasing cells were fabricated using thin silicon wafers (200 μm, 4-inches, undoped) purchased from Virginia Semiconductor (Fredericksburg, VA). Low stress silicon nitride membranes of 35 nm in thickness were deposited on the silicon wafer, which form the viewing window of a biasing cell.

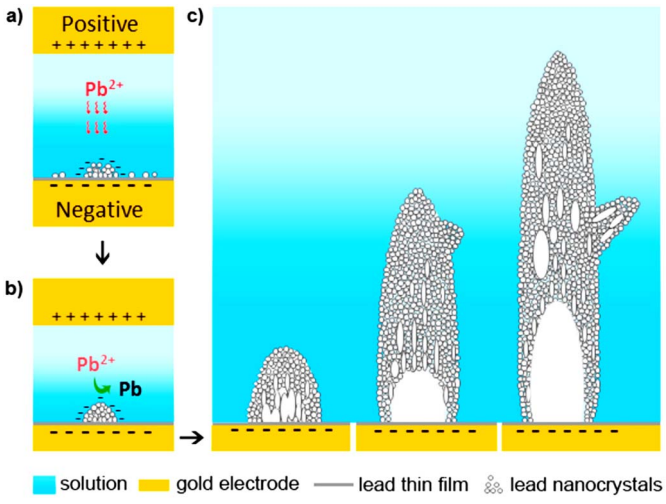

Figure 6 | A cartoon showing the electrochemical growth of lead dendrites. It illustrates the proposed growth model that the reduced metal ions form a cluster with nanograins and with polycrystalline features. The growth of a single crystal branch is achieved by the alignment and attachment of nanograins. Note: this cartoon was drawn by KN using an Adobe Photoshop software.

The dimensions of a view window are 25 μm × 6 μm. A series of photolithography patterning and etching processes were incorporated to generate the viewing window and two reservoirs of a biasing cell. On the bottom chip two 100 nm-thick gold electrodes are patterned and sputtered on the window with a face-to-face distance of 20 μm across the viewing window. The bottom and top chips were aligned manually and assembled together by a 150 nm thick indium spacer. Gold nanowires were bonded onto gold electrode pads of the liquid cell (Figure 1(b)) and they were connected to the copper wires of the TEM holder. After liquid loading, we sealed the cell and loaded the sample into the microscope for in situ experiments. Except the fabrication of electrodes and wire bonding, all other processes can be found in the previous publications[23,24]. The electrochemical process was controlled by an electrochemical workstation (Model 660D series made by CH Instruments). The liquid solution of lead nitrate dissolved in triethylene glycol and water (100 mg/mL and 5 mg/mL) was loaded into reservoirs with a syringe. Liquid flows into the cell by capillary force. The ratio of triethylene glycol to water varied from 4 : 1 to 3 : 2. Videos of the electrochemical reactions were recorded at 8 frames per second although faster recording is available for the set up. In this work, only two electrodes were used for the ease of cell fabrication as the initial effort. However, a third reference electrode is allowed in the electrochemical cell design and set up. A JOEL 2100 TEM operated at 200 kV was used for the in situ electrochemical TEM experiments. Electron beam density of about 5×10^2 electrons$\cdot s^{-1}\cdot Å^{-2}$ was maintained during image recording. Some ex situ TEM images were taken using a FEI Tecnai T20 operated at 200 kV.

1. Aurbach, D., Zinigrad, E., Cohen, Y. & Teller, H. A short review of failure mechanisms of lithium metal and lithiated graphite anodes in liquid electrolyte solutions. *Solid State Ionics* **148**, 405–416, doi:10.1016/s0167-2738(02)00080-2 (2002).
2. Devaney, J. R. Packing and corrosion – corrosion and dendrite growth. *Microprocess. Microprogr.* **19**, 427–427 (1987).
3. Tiller, W. A. Dendrites: Understanding of this familiar phenomenon has led to the development of useful man-made materials. *Science* **146**, 871–879, doi:10.1126/science.146.3646.871 (1964).
4. Ogburn, F., Bechtoldt, C., Morris, J. B. & de Koranyi, A. Structure of electrodeposited lead dendrites. *Journal of The Electrochemical Society* **112**, 574–577, doi:10.1149/1.2423609 (1965).
5. Langer, J. S. Dendrites, vscous fingers, and the theory of pattern formation. *Science* **243**, 1150–1156, doi:10.1126/science.243.4895.1150 (1989).
6. Miyata, Y., Glicksman, M. E. & Tirmizi, S. H. Dendritic growth with interfacial energy anisotropy. *Journal of Crystal Growth* **110**, 683–691, doi:http://dx.doi.org/10.1016/0022-0248(91)90624-E (1991).
7. Mogi, I., Okubo, S. & Nakagawa, Y. Effect of high magnetic fields on fractal growth of lead metal-leaves. *Journal of Crystal Growth* **128**, 258–261, doi:http://dx.doi.org/10.1016/0022-0248(93)90329-U (1993).
8. Trivedi, R. & Kurz, W. Dendritic Growth. *Int. Mater. Rev.* **39**, 49–74 (1994).
9. Libbrecht, K. G. & Tanusheva, V. M. Electrically induced morphological instabilities in free dendrite growth. *Phys. Rev. Lett.* **81**, 176–179 (1998).
10. Borzsonyi, T., Toth-Katona, T., Buka, A. & Granasy, L. Dendrites regularized by spatially homogeneous time-periodic forcing. *Phys. Rev. Lett.* **83**, 2853–2856, doi:10.1103/PhysRevLett.83.2853 (1999).

11. Boettinger, W. J. *et al.* Solidification microstructures: Recent developments, future directions. *Acta Mater.* **48**, 43–70, doi:10.1016/s1359-6454(99)00287-6 (2000).
12. Qiao, J. W. In-situ dendrite/metallic glass matrix composites: a review. *J. Mater. Sci. Technol.* **29**, 685–701, doi:10.1016/j.jmst.2013.05.020 (2013).
13. Liaw, H. M. & Faust Jr, J. W. Effect of growth parameters on habit and morphology of electrodeposited lead dendrites. *Journal of Crystal Growth* **18**, 250–256, doi:http://dx.doi.org/10.1016/0022-0248(73)90168-1 (1973).
14. Kraus, T. & de Jonge, N. Dendritic gold nanowire growth observed in liquid with transmission electron microscopy. *Langmuir* **29**, 8427–8432, doi:10.1021/la401584z (2013).
15. Granasy, L., Pusztai, T., Borzsonyi, T., Warren, J. A. & Douglas, J. F. A general mechanism of polycrystalline growth. *Nat. Mater.* **3**, 645–650, doi:10.1038/nmat1190 (2004).
16. Fang, J. X. *et al.* Double-interface growth mode of fractal silver trees within replacement reaction. *Appl. Phys. Lett.* **89**, doi:17310410.1063/1.2364057 (2006).
17. Shen, Q. M. *et al.* Three-dimensional dendritic Pt nanostructures: sonoelectrochemical synthesis and electrochemical applications. *J. Phys. Chem. C* **112**, 16385-16392, doi:10.1021/jp8060043 (2008).
18. Cheng, Y., Wang, Y. S., Chen, D. & Bao, F. Evolution of single crystalline dendrites from nanoparticles through oriented attachment. *J. Phys. Chem. B* **109**, 794–798, doi:10.1021/jp0460240 (2005).
19. Chen, X., Noh, K. W., Wen, J. G. & Dillon, S. J. In situ electrochemical wet cell transmission electron microscopy characterization of solid-liquid interactions between Ni and aqueous NiCl2. *Acta Mater.* **60**, 192–198, doi:10.1016/j.actamat.2011.09.047 (2012).
20. Williamson, M. J., Tromp, R. M., Vereecken, P. M., Hull, R. & Ross, F. M. Dynamic microscopy of nanoscale cluster growth at the solid-liquid interface. *Nat. Mater.* **2**, 532–536, doi:10.1038/nmat944 (2003).
21. White, E. R. *et al.* In Situ transmission electron microscopy of lead dendrites and lead ions in aqueous solution. *ACS Nano* **6**, 6308–6317, doi:10.1021/nn3017469 (2012).
22. Chen, X., Zhou, L. H., Wang, P., Zhao, C. J. & Miao, X. L. A Study of nano materials and their reactions in liquid using in situ wet cell TEM technology. *Chin. J. Chem.* **30**, 2839–2843, doi:10.1002/cjoc.201201036 (2012).
23. Zheng, H. *et al.* Observation of Single Colloidal Platinum Nanocrystal Growth Trajectories. *Science* **324**, 1309–1312, doi:10.1126/science.1172104 (2009).
24. Liao, H.-G., Cui, L., Whitelam, S. & Zheng, H. Real-Time Imaging of Pt3Fe Nanorod Growth in Solution. *Science* **336**, 1011–1014, doi:10.1126/science.1219185 (2012).
25. Woehl, T. J., Evans, J. E., Arslan, I., Ristenpart, W. D. & Browning, N. D. Direct in situ determination of the mechanisms controlling nanoparticle nucleation and growth. *ACS Nano* **6**, 8599–8610, doi:10.1021/nn303371y (2012).
26. White, E. R., Mecklenburg, M., Singer, S. B., Aloni, S. & Regan, B. C. Imaging nanobubbles in water with scanning transmission electron microscopy. *Applied Physics Express* **4**, doi:05520110.1143/apex.4.055201 (2011).
27. Woehl, T. J. *et al.* Experimental procedures to mitigate electron beam induced artifacts during in situ fluid imaging of nanomaterials. *Ultramicroscopy* **127**, 53–63, doi:10.1016/j.ultramic.2012.07.018 (2013).
28. Longo, E. *et al.* Direct in situ observation of the electron-driven synthesis of Ag filaments on α-Ag_2WO_4 crystals. *Sci. Rep.* **3**, 1676; DOI:10.1038/srep01676 (2013).

Acknowledgments

The in situ TEM experiments were conducted using MSD TEM facility at Lawrence Berkeley National Laboratory. We performed part of ex situ TEM experiments at National Center for Electron Microscopy (NCEM) of the Lawrence Berkeley National Laboratory (LBNL), which is supported by the U.S. Department of Energy (DOE) under Contract # DE-AC02-05CH11231.

Author contributions

M.S., H.L. and K.N. performed experiments. K.N. prepared the figures. H.Z. designed the experiments and perceived the work. All authors participated in data analysis and writing the manuscript. All authors reviewed the manuscript.

Additional information

Supplementary information accompanies this paper at http://www.nature.com/scientificreports

Competing financial interests: The authors declare no competing financial interests.

How to cite this article: Sun, M.H., Liao, H.-G., Niu, K.Y. & Zheng, H.M. Structural and Morphological Evolution of Lead Dendrites during Electrochemical Migration. *Sci. Rep.* **3**, 3227; DOI:10.1038/srep03227 (2013).